

Mixing from Fickian Diffusion and Natural Convection in Binary Non-Equilibrium Fluid Phases

L. Rongy, K. B. Haugen, and A. Firoozabadi

Dept. of Chemical Engineering, Mason Laboratory, Yale University, New Haven, CT 06511

DOI 10.1002/aic.12685

Published online June 16, 2011 in Wiley Online Library (wileyonlinelibrary.com).

A two-dimensional (2-D) model that describes mass transport between non equilibrium gas and liquid phases of a binary non polar mixture in a closed system of fixed volume and temperature is presented. Diffusion, convective mass transport due to compressibility and non ideality, and the motion of the interface upon evaporation and dissolution are accounted. Natural convection in both phases is incorporated, which allows to study the effect of density increase in the liquid phase from gas dissolution. The Peng-Robinson equation of state is used to calculate the densities and the fugacities needed to find the interfacial composition consistent with local chemical equilibrium. The results obtained with a one-dimensional model was compared to our 2-D results, showing that natural convection influences the mixing time drastically. In the liquid bulk phase, convective flux is much higher than diffusive flux. Across the interface, diffusive flux is, however, the dominating flux, which allows accurate measurement of diffusion coefficients at high pressure in 2-D domains. © 2011 American Institute of Chemical Engineers *AICHE J*, 58: 1336–1345, 2012

Keywords: two-phase systems, mixing, carbon dioxide, density-driven flow, diffusion coefficients

Introduction

The mixing of two non equilibrium fluid phases is relevant to a large number of applications such as improved oil recovery and carbon sequestration.

Gas injection into oil reservoirs has long been used to maintain the pressure needed for recovery processes. The subsequent mixing between the gas and the liquid phase affects the physical properties of the oil such as its viscosity, density, and surface tension.¹ As a result, the recovery process might become more efficient, which is referred to as secondary recovery mechanisms.

Reducing greenhouse gas emissions to hold back climate changes represents one of the most important challenges of our time. Underground injection of carbon dioxide (CO₂) in geological formations is a promising method considered for sequestering CO₂ captured from fossil-fuel power plants to reduce its concentration in the atmosphere and, therefore, its impact on global warming and climate change.^{2,3} Different geological sites, including depleted oil fields, abandoned mining operations, saline aquifers, and deep-sea sediments have been proposed as possible long-term storage locations for CO₂. At those underground conditions, CO₂ increases the density of the liquid present in the geological formation, which may lead to natural convection affecting the mixing processes.

A large number of studies have examined the onset of convection during the mixing of CO₂ and brine in porous media both experimentally and with theoretical and

Correspondence concerning this article should be addressed to A. Firoozabadi at abbas.firoozabadi@yale.edu.

Current Address of L. Rongy: Center for Nonlinear Phenomena and Complex Systems, Université Libre de Bruxelles, CP231, B-1050 Brussels, Belgium.

numerical models, often with the assumption of fixed interface conditions.⁴⁻⁷

The mixing between CO₂ and water was recently studied experimentally in a pressure volume temperature (PVT) cell⁸ and a model was proposed to account for natural convection. However, to the best of our knowledge, there is no work in the literature describing the mixing between two non equilibrium fluid phases and including natural convection in both phases as well as the motion of the interface upon the phase changes.

Our purpose is two-fold. First, our work provides a realistic description of the mixing processes, which is needed to assess the efficiency of oil extraction and the storage capacity in geological formations. In particular, we provide further insight into the dynamics of mixing between CO₂ and a hydrocarbon liquid phase, highlighting the role of the different transport processes and the time scales of the system. Second, we are able to infer accurate diffusion coefficients from measurements such as pressure evolution and gas-liquid level data by comparing the results obtained with our model to these experimental data.

The article is organized as follows. In the next section, we present the two-dimensional (2-D) governing equations describing the compositional changes arising from Fickian diffusion and convective mass transport. The motion of the interface upon mixing is incorporated in the model formulation, and the velocity field is described by the compressible Navier-Stokes equations. The interfacial and boundary conditions as well as the numerical integration method are also presented. Next, we focus on the mixing between CO₂ and liquid normal decane (nC₁₀), comparing our results with experimental data (from Instituto Mexicano del petroleo) and measuring the diffusion coefficient accurately. The influence of the diffusion coefficient and of natural convection are next investigated and the non linear transient dynamics is analyzed before concluding the work in the last section.

Physical Model

The set up we study theoretically and numerically is a 2-D PVT cell with constant volume and temperature (see Figure 1). In experiments, the cell is partly filled with liquid and the remainder is filled with gas. As the two phases equilibrate, the pressure and the liquid level change in time. Across the interface, local thermodynamic equilibrium is assumed. As a consequence, the composition on either side of the interface differs from the composition of the bulk phases. This triggers mass transport by diffusive motion and by advection with a bulk velocity arising from compressibility, non ideality, and natural convection if the system is buoyantly unstable.

The gas-liquid interface is perpendicular to the gravity field and, as the two phases mix, it can move upward or downward. We assume, however, that the interface remains flat. This assumption of non deformability rests on the fact that surface tension dominates over pressure and normal viscous stresses in the normal momentum balance at the interface.⁹ A suitably defined capillary number is shown to be small. We also neglect variations in surface tension along the interface, which is a good assumption for the mixing between non reactive binary phases. We comment further on this assumption toward the end of this section.

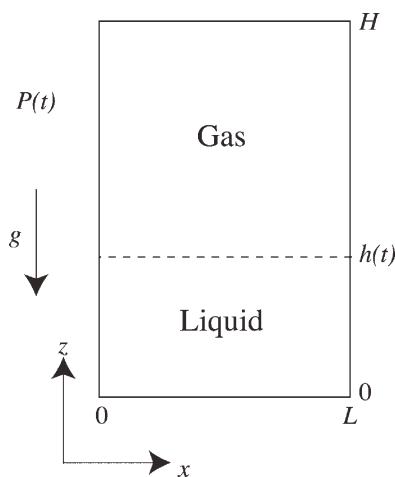


Figure 1. Sketch of a PVT cell with constant volume and temperature.

H is the total height and *L* is the width of the cell. The gas-liquid interface is perpendicular to the gravity field \vec{g} and the pressure *P* and liquid level *h* vary with time as the two phases mix.

The governing equations in both phases are derived from local mass and momentum balances.

Mass and Component Balance

The total mass balance is expressed by the continuity equation as

$$\frac{\partial \rho}{\partial t} + \nabla \cdot (\rho \vec{v}) = 0 \quad (1)$$

where for each phase, ρ is the mass density, *t* is the time, and $\vec{v} = (u, w)$ is the 2-D velocity field. The composition of each phase is determined by the mass fraction ω of one of the two components that we call component 1, component 2 being treated as the reference component. Writing the local component balance yields

$$\rho \left(\frac{\partial \omega}{\partial t} + \vec{v} \cdot \nabla \omega \right) = -\nabla \cdot \vec{J} \quad (2)$$

where \vec{J} is the Fickian diffusive mass flux of component 1 in the corresponding phase, expressed as

$$\vec{J} = -\rho D \nabla \omega \quad (3)$$

Pressure diffusion effects are neglected and the diffusion coefficient *D* is calculated as a function of pressure and composition.¹⁰ A detailed explanation for the calculation of *D* is given further. As the mixing process is assumed isothermal, the density is a function of pressure *P* and composition. Using the chain rule to expand the derivatives of density in Eq. 1 leads to

$$\frac{\partial \rho}{\partial P} \left(\frac{\partial P}{\partial t} + \vec{v} \cdot \nabla P \right) + \frac{\partial \rho}{\partial \omega} \left(\frac{\partial \omega}{\partial t} + \vec{v} \cdot \nabla \omega \right) + \rho \nabla \cdot \vec{v} = 0 \quad (4)$$

We suppose that the spatial variations in pressure have a negligible effect on the density field. This assumption is

justified for the problem discussed in this article. Rearranging Eq. 4 and using Eq. 2 lead to the following expression for the divergence of the velocity field

$$\nabla \cdot \vec{v} = -\frac{1}{\rho} \frac{\partial \rho}{\partial P} \frac{\partial P}{\partial t} + \frac{1}{\rho^2} \frac{\partial \rho}{\partial \omega} \nabla \cdot \vec{J} \quad (5)$$

Equation 5 indicates that compressibility and non ideality (density variations with composition) can both be sources of divergence of the velocity field. To fully determine \vec{v} , we obtain evolution equations from the momentum balance in the next section.

Momentum Balance

We consider both the gas and the liquid phases to be Newtonian fluids and active in terms of convection. We can, therefore, write the momentum equations in each phase

$$\rho \left(\frac{\partial \vec{v}}{\partial t} + \vec{v} \cdot \nabla \vec{v} \right) = \rho \vec{g} - \nabla P + \mu \nabla^2 \vec{v} + \left(\kappa + \frac{\mu}{3} \right) \nabla (\nabla \cdot \vec{v}), \quad (6)$$

where μ and κ are the shear viscosity and the bulk viscosity, respectively, assumed to be constant within each phase, and \vec{g} is the gravity field. After linearizing and subsequently taking the curl of Eq. 6 within the Boussinesq approximation, we obtain the following expression for the curl of the velocity field

$$\frac{\partial}{\partial t} (\nabla \times \vec{v}) = \frac{g}{\rho} \frac{\partial \rho}{\partial x} + \frac{\mu}{\rho} \nabla^2 (\nabla \times \vec{v}) \quad (7)$$

corresponding to a diffusion equation for the vorticity field with a source term arising from density gradients. The density field in the buoyancy term is evaluated as a function of pressure and composition using the Peng-Robinson equation of state appropriate to the non polar mixtures considered here.¹¹

Interfacial and Boundary Conditions

The exchange of mass between the gas and liquid phases is by condensation and evaporation, which are fast processes compared to the time scale over which mixing processes occur. To determine the composition of the interface, denoted by its position $z = h(t)$ varying with time, we make the assumption of local thermodynamic equilibrium, by invoking the equality of the fugacity f_i of each component i across the interface

$$f_i^G(T, P, \omega^G) = f_i^L(T, P, \omega^L), \quad z = h(t) \quad \text{for } i = 1, 2 \quad (8)$$

where the superscripts G and L denote the gas and liquid phases, respectively. Like the densities in the governing equations, the fugacities are calculated as a function of temperature T (constant throughout this article), pressure, and composition using the Peng-Robinson equation of state.¹¹ Eq. 8 is solved for ω^G and ω^L that are, therefore, functions of temperature and pressure only. As the temperature is constant everywhere and we have assumed the equation of state is not affected by the spatial variations of pressure appreciably, the composition is uniform along the interface. We note that this is only true for a binary system for which the number of unknown compositions

at the interface matches the number of equations describing the interfacial chemical equilibrium. This enforces our assumption that the surface tension does not vary along the interface.

The vertical velocity at both sides of the interface is obtained by imposing the continuity of the mass fluxes. The total mass balance across the interface yields

$$\rho^G \left(w^G - \frac{\partial h}{\partial t} \right) = \rho^L \left(w^L - \frac{\partial h}{\partial t} \right), \quad z = h(t) \quad (9)$$

where $\partial h / \partial t$ is the rate of change in liquid level accounting for the moving interface. In the absence of any chemical reactions, the mass flux of each component is also continuous across the interface, leading to an additional equation for the conservation of the mass flux of component 1

$$\rho^G \omega^G \left(w^G - \frac{\partial h}{\partial t} \right) + J_z^G = \rho^L \omega^L \left(w^L - \frac{\partial h}{\partial t} \right) + J_z^L, \quad z = h(t) \quad (10)$$

where J_z is the vertical diffusive flux. The vertical velocities at the interface, $w^G(x, z = h(t))$ and $w^L(x, z = h(t))$, are obtained by solving Eqs. 9 and 10.

We assume that the horizontal velocities are continuous at the interface, $u^G(x, z = h(t)) = u^L(x, z = h(t))$, and the tangential momentum balance across the interface allows to determine them uniquely

$$\begin{aligned} \mu^G \left(\frac{\partial u^G}{\partial z} + \frac{\partial w^G}{\partial x} \right) - \mu^L \left(\frac{\partial u^L}{\partial z} + \frac{\partial w^L}{\partial x} \right) \\ = \rho^G u^G \left(w^G - \frac{\partial h}{\partial t} \right) - \rho^L u^L \left(w^L - \frac{\partial h}{\partial t} \right) \end{aligned} \quad (11)$$

We note that Eq. 9 and the assumption of continuity of horizontal velocities across the interface force the right-hand side of Eq. 11 to become zero. One may replace the continuity of horizontal velocities (i.e. tangential velocities) by the continuity of normal viscous shear stresses across the interface, leading to the following relationship between the velocities at both sides of the interface, $\mu^G u^G(x, z = h(t)) = \mu^L u^L(x, z = h(t))$ and leaving the right-hand side of Eq. 11 non zero. We have examined both the slip and the no-slip boundary conditions. For the viscosity ratio between the gas and the liquid phases we consider here ($\mu^L / \mu^G \sim 44$, see Table 1), those two sets of boundary conditions give nearly similar results. However, the intensity of convection in the gas phase depends on the interfacial set of conditions and the differences observed increase with the viscosity ratio.

At the four impermeable walls, we use no-slip and no-flux boundary conditions for the velocities and the composition, respectively

$$J_x^G = 0 = u^G = w^G, \quad x = 0, L \quad \text{and } z \geq h(t) \quad (12)$$

$$J_x^L = 0 = u^L = w^L, \quad x = 0, L \quad \text{and } z \leq h(t) \quad (13)$$

$$J_z^G = 0 = u^G = w^G, \quad \forall x \quad \text{and } z = H \quad (14)$$

$$J_z^L = 0 = u^L = w^L, \quad \forall x \quad \text{and } z = 0 \quad (15)$$

where L is the width of the system and H its total height.

Table 1. Critical Temperatures (T_c) and Pressures (P_c), Acentric Factors (λ), Volume Shift Parameters (c), Molecular Weights (MW), Shear Viscosities (μ), Diffusion Volumes (V_f), and Binary Interaction Parameter (k_{12}) Used in the Volume-Translated Peng-Robinson Equation of State¹¹ and in the Diffusion Coefficients Correlation¹⁰

	T_c (K)	P_c (10^5 Pa)	λ	c	MW (g/mol)	$\mu(10^{-5}$ Pa s)	V_f	k_{12}
CO ₂	304.1	73.75	0.239	0.1137	44.01	1.606	26.9	
nC ₁₀	617.7	21.10	0.489	0.0865	142.3	71.26	209.8	0.123

The volume shift parameters and the binary interaction parameter have been fitted using independent experimental data on a CO₂-nC₁₀ mixture.¹⁶

Numerical Implementation

The numerical scheme developed to integrate the equations presented above uses a finite-volume discretization and builds on the work by Haugen and Firoozabadi.^{12,13} In the numerical implementation, we use a reference frame centered on and moving with the interface. The volume element is rectangular because a higher precision is needed in the vertical direction to describe the transport processes across the interface accurately.

The integration starts by performing an interfacial flash to predict the interfacial composition using Eq. 8 and the interfacial vertical velocities using Eqs. 9–10. The velocity field in each phase, $\partial P/\partial t$, and $\partial h/\partial t$ are next found by solving the linear set of equations formed by Stokes' theorem applied to the integral form of Eq. 5 and Green's theorem applied to each volume element. Eqs 2 and 7 are then integrated using an explicit Euler formulation. The density field and the diffusion coefficients are updated with the new composition and pressure fields. The next step consists of moving the boundaries by $\partial h/\partial t$ and adjusting the mesh accordingly. The details on how the changes in size of the gas and liquid domains are numerically implemented can be found in Appendix A of Haugen and Firoozabadi.¹²

We have validated our numerical integrations by reproducing results previously obtained with a one-dimensional (1-D) code.¹² Besides, our numerical solutions were found to converge on decreasing the size of the volume elements and the time step. A typical grid size used in this article is 1200×30 to represent a 12-cm long and 19-mm wide system. The time step is chosen adaptively between 5.5×10^{-6} and 5.5×10^{-3} s by comparing the local changes in time of the variables with the magnitude of the global changes and is not allowed to increase by more than 5% between two iterations.

Mixing dynamics: CO₂-nC₁₀ Mixture

In the remainder of this article, we will mainly consider the mixing between CO₂, which we will refer to as component 1, and normal decane, which we will treat as the reference component. To compute the densities and the fugacities, we use the volume-translated Peng-Robinson equation of state¹¹ (see Table 1 for related input parameters).

Measurement of the Diffusion Coefficient

The diffusion coefficient D varies with space and time because of the changes in composition and pressure. We update the diffusion coefficient at the interface and in each volume element of our numerical grid every 5 s. We have tested that more frequent updates lead to the same results.

To account for the dependence of D on pressure and composition, we use the unified model for non ideal and non polar multicomponent mixtures developed by Leahy-Dios and Firoozabadi.¹⁰ An empirical correlation is first used to predict the binary infinite-dilution diffusion coefficients, $D_{12}^\infty(T,P)$ (corresponding to CO₂ infinitely diluted in nC₁₀) and $D_{21}^\infty(T,P)$ (corresponding to nC₁₀ infinitely diluted in CO₂). Further dependence on temperature, pressure, and composition is then calculated using the Vignes relation and an accurate description of the mixture non ideality by the fugacity derivatives evaluated with the Peng-Robinson equation of state^{10,11,14} (see Table 1 for related input parameters).

We compare our numerical integrations with experimental data (from Instituto Mexicano del petroleo) obtained in a cylindrical PVT cell containing a CO₂-nC₁₀ mixture at $T = 313.1$ K. The height of the cell, H , is equal to 12 cm and its diameter, corresponding to our variable L , is equal to 19 mm. The small cell diameter, along with the fact that the cell is placed in an isothermal bath, justify the assumption that the mixing processes can be treated as isothermal. The initial condition consists of pure gaseous CO₂ on top of pure liquid normal decane. The initial pressure is 40.1×10^5 Pa, and the initial liquid level is 3.48 cm. Upon dissolution of CO₂ into the liquid phase, the pressure decreases. Figure 2a shows that using the correlation described above for the diffusion coefficients overestimates the rate of pressure change. The corresponding diffusion coefficients at the interface and in the bulk phases are presented in Table 2, for the initial condition, when the bulk phases are uniform, and at the final condition. Table 2 also shows the initial and final infinite-dilution diffusion coefficients, varying with time due to the pressure changes. The discrepancy between the experimental data and the theoretical results observed in Figure 2a can be due to either the representation of a cylinder by 2-D Cartesian coordinates or to the correlation used for the mixture of CO₂ and normal decane. We note that, as D_{12}^∞ increases by only 2% during the experiment, we can treat it as a constant fitting parameter and use our model to measure its value.

We have first tested that using a constant D_{12}^∞ equal to either its value at the initial pressure or its value at the final pressure both lead to the same result as using the value predicted by the correlation and changing in time with pressure. We have next found that, for the experimental conditions, the optimal $D_{12}^\infty = 1.7 \times 10^{-9}$ m²/s (see Figure 2a). Table 3 gives the corresponding initial and final D^G and D^L . Their temporal and spatial dependences at the interface and through the bulk will be presented further in this section. Figure 2b shows the increase in liquid level arising from the dissolution of CO₂ in the liquid phase. No experimental data are available for the liquid level evolution of this system to compare with our simulations.

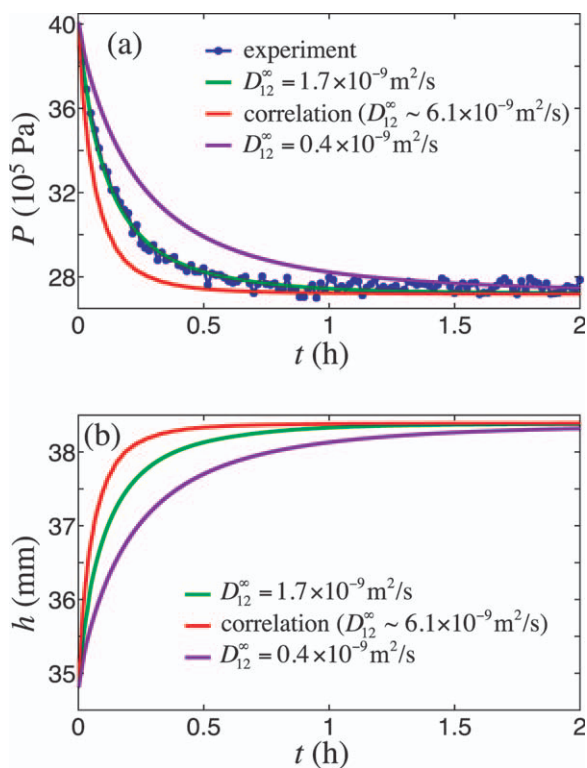


Figure 2. Pressure (a) and liquid level (b) as a function of time with diffusion coefficients varying in time.

The diffusion coefficient at infinite dilution of CO_2 in $n\text{C}_{10}$, D_{12}^∞ , predicted by the correlation evolves from 6.04×10^{-9} to $6.16 \times 10^{-9} \text{ m}^2/\text{s}$, whereas the comparison with experimental data shows that the optimal $D_{12}^\infty = 1.7 \times 10^{-9} \text{ m}^2/\text{s}$. The temperature is constant, $T = 313.1 \text{ K}$, the initial pressure $P_0 = 40.1 \times 10^5 \text{ Pa}$, the initial liquid level $h_0 = 3.48 \text{ cm}$, and the system dimensions are $H = 12 \text{ cm}$ and $L = 19 \text{ mm}$. [Color figure can be viewed in the online issue, which is available at wileyonlinelibrary.com.]

The data for the pressure changes can also be fitted with constant effective diffusion coefficients, $D^G = 1.5 \times 10^{-7} \text{ m}^2/\text{s}$ and $D^L = 5.6 \times 10^{-9} \text{ m}^2/\text{s}$ (see Figure 3). Those values are only valid for the particular experimental set-up we are considering here as they constitute an effective measure of the diffusive transport process throughout the experiment.

Table 2. Initial ($t = 0$) and Final ($t = t_\infty$) Diffusion Coefficients in the Gas and Liquid Phases, D^G and D^L , respectively, calculated using the correlation from Leahy-Dios and Firoozabadi.¹⁰

	$t = 0$	$t = t_\infty$
$D_{\text{interface}}^G$ ($\times 10^{-7} \text{ m}^2/\text{s}$)	1.05	1.70
D_{bulk}^G ($\times 10^{-7} \text{ m}^2/\text{s}$)	1.06	
$D_{\text{interface}}^L$ ($\times 10^{-8} \text{ m}^2/\text{s}$)	1.46	1.35
D_{bulk}^L ($\times 10^{-8} \text{ m}^2/\text{s}$)	0.604	
D_{12}^∞ ($\times 10^{-9} \text{ m}^2/\text{s}$)	6.04	6.16
D_{21}^∞ ($\times 10^{-7} \text{ m}^2/\text{s}$)	1.06	1.71

The infinite-dilution coefficients, D_{12}^∞ and D_{21}^∞ , also change during the mixing because of the decrease in pressure. The values in the table have been calculated for a CO_2 - $n\text{C}_{10}$ mixture at $T = 313.1 \text{ K}$, with the initial pressure $P_0 = 40.1 \times 10^5 \text{ Pa}$, the initial liquid level $h_0 = 3.48 \text{ cm}$, and the system dimensions $H = 12 \text{ cm}$ and $L = 19 \text{ mm}$.

Table 3. Initial ($t = 0$) and Final ($t = t_\infty$) Diffusion Coefficients in the Gas and Liquid Phases, D^G and D^L , respectively, Calculated from a Constant $D_{12}^\infty = 1.7 \times 10^{-9} \text{ m}^2/\text{s}$ and using the correlation from Leahy-Dios and Firoozabadi¹⁰ for D_{21}^∞

	$t = 0$	$t = t_\infty$
$D_{\text{interface}}^G$ ($\times 10^{-7} \text{ m}^2/\text{s}$)	1.05	1.70
D_{bulk}^G ($\times 10^{-7} \text{ m}^2/\text{s}$)	1.06	
$D_{\text{interface}}^L$ ($\times 10^{-9} \text{ m}^2/\text{s}$)	6.78	5.33
D_{bulk}^L ($\times 10^{-9} \text{ m}^2/\text{s}$)	1.70	

The other parameters are the same as in Table 2.

We point out that, in both Figures 2 and 3, the results are very sensitive to D_{12}^∞ and D^L , respectively. The time needed to reach equilibrium decreases when the diffusion coefficient increases, leading to a faster mixing. On the contrary, changing the diffusion coefficient in the gas phase by a factor of 2 does not influence the results significantly. This is because, for these experimental conditions, the composition of the gas phase remains almost pure CO_2 with very little normal decane evaporating. The maximum mass fraction of $n\text{C}_{10}$ in the gas phase is indeed only 0.2% at equilibrium.

Influence of Natural Convection

Upon dissolution, CO_2 increases locally the density of the liquid phase leading to a buoyantly unstable situation. The local unstable density gradient along with numerical fluctuations (we did not perturb the system in any specific way) triggers natural convection. The influence of convection on the mixing time scale is shown in Figure 4 where we compare the predictions of a 1-D model^{12,13} with our 2-D results for constant diffusion coefficients. We use the optimal liquid diffusion coefficient found in Figure 3, $D^L = 5.6 \times 10^{-9} \text{ m}^2/\text{s}$ and observe that it takes approximately 100 h to reach the equilibrium with a 1-D model not accounting for natural convection whereas it only takes 2 h in the experiment (see Figure 4a). We also compare the dynamics of the CO_2 - $n\text{C}_{10}$ system with a methane (CH_4)- $n\text{C}_{10}$ mixture. In the former case, the density increase in the liquid phase amounts

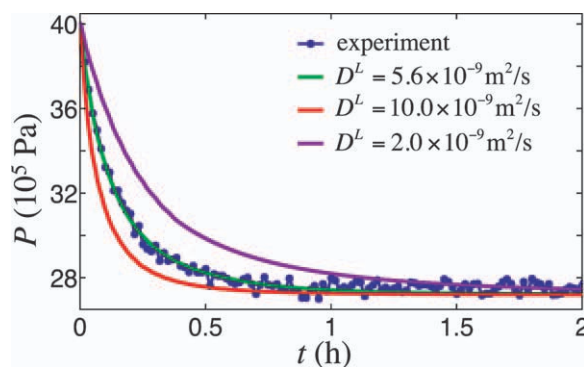


Figure 3. Pressure as a function of time for different constant diffusion coefficients in the liquid phase, D^L .

The optimal $D^L = 5.6 \times 10^{-9} \text{ m}^2/\text{s}$ and the diffusion coefficient in the gas phase, D^G , is equal to $1.5 \times 10^{-7} \text{ m}^2/\text{s}$ for all the plots. The other parameters are the same as in Figure 2. [Color figure can be viewed in the online issue, which is available at wileyonlinelibrary.com.]

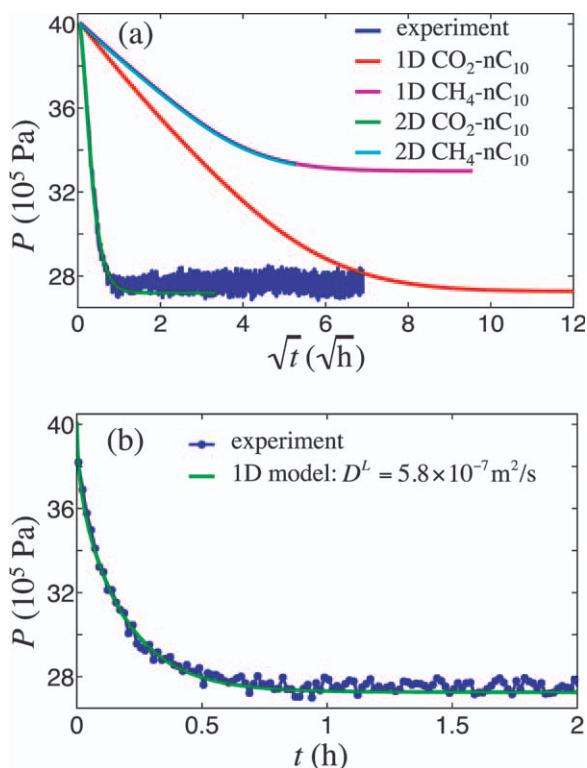


Figure 4. Comparison between the predictions of a 1-D model^{12,13} and our 2-D model with constant diffusion coefficients.

(a) Pressure as a function of the square root of time using a 1-D and a 2-D model: for the CO_2 - nC_{10} system, $D^L = 5.6 \times 10^{-9} \text{ m}^2/\text{s}$ and $D^G = 1.5 \times 10^{-7} \text{ m}^2/\text{s}$; for the CH_4 - nC_{10} system, $D^L = 1.25 \times 10^{-8} \text{ m}^2/\text{s}$ and $D^G = 2.49 \times 10^{-7} \text{ m}^2/\text{s}$, values obtained by using the correlation for diffusion coefficients at the equilibrium conditions.¹¹ The binary interaction parameter between CH_4 and nC_{10} is 0.045 and the additional parameters are taken from Haugen and Firoozabadi.^{12,13} (b) Pressure as a function of time fitted by a 1-D model with $D^L = 5.8 \times 10^{-7} \text{ m}^2/\text{s}$ and $D^G = 1.5 \times 10^{-7} \text{ m}^2/\text{s}$. The mixture is formed by CO_2 and nC_{10} , and temperature, initial conditions, and system dimensions are the same as in Figure 2. [Color figure can be viewed in the online issue, which is available at wileyonlinelibrary.com.]

to 0.01 g/cm^3 at the end of the mixing whereas in the latter case, there is no density increase of the liquid phase upon dissolution of methane. This explains why, in that case, the results of the 1-D model are identical to the ones of the 2-D model (see Figure 4a). We note that the mixing in the (CH_4) - nC_{10} system occurs on the same time scale as the mixing in the CO_2 - nC_{10} system without natural convection. Using a 2-D code accounting for natural convection is crucial as the experimental data can also be fitted with a 1-D model but the predicted D^L is two orders of magnitude higher in that case (see Figure 4b). We would like to repeat that in our article we have used a 2-D numerical Cartesian coordinate model for the study of a cylindrical geometry. The numerical model is expected to capture the essence of gravity effect. In the future, we plan to verify our model with composition and velocity data as they become available in the literature.

Figures 5 and 6 show the evolution of the composition at the interface and in the liquid phase. The interfacial mass

fraction of dissolved CO_2 is maximum at the initial pressure. Following the dissolution of CO_2 in the liquid phase, the pressure decreases, which leads to lower concentrations of CO_2 dissolved at the interface. The concentration of CO_2 at the liquid side of the interface follows the drop in pressure (see Figure 5). For the sake of clarity, the results are presented in the frame of the moving interface, located at $z = 0$ in all the graphs below. The liquid concentration of CO_2 is maximum at the interface and drops sharply below the interface to become almost uniform in the bulk (see Figure 6). This points out that the dissolved CO_2 is rapidly taken away from the interface by convection and mixed in the bulk phase with a very efficient mixing rate. Figure 6 pictures the rapid build-up of CO_2 concentration in the liquid bulk phase. In the gas phase, there is only a small reduction in the concentration of CO_2 . We do not show the results for brevity.

The changes in pressure and composition discussed above affect the diffusion coefficients at the interface and in the bulk phases. Composition has a stronger effect than pressure on the diffusion coefficient in the liquid phase, whereas, in the gas phase, D^G is affected almost by pressure only, as expected because of the small composition changes. Eventually, we note that the diffusion coefficients are almost uniform within each bulk phases, except close to the liquid side of the interface.

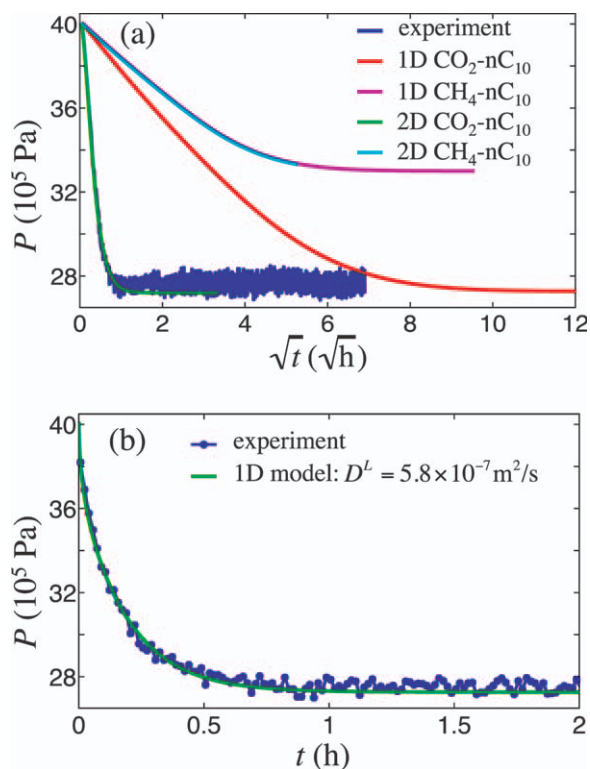


Figure 5. Interfacial composition of CO_2 on the liquid side as a function of (a) time and (b) pressure.

Binary interfacial compositions depend on T and P only and are, therefore, uniform along the interface in our system. The diffusion coefficients are calculated as a function of pressure and composition using $D_{12}^\infty = 1.7 \times 10^{-9} \text{ m}^2/\text{s}$, and the other parameters are the same as in Figure 2.

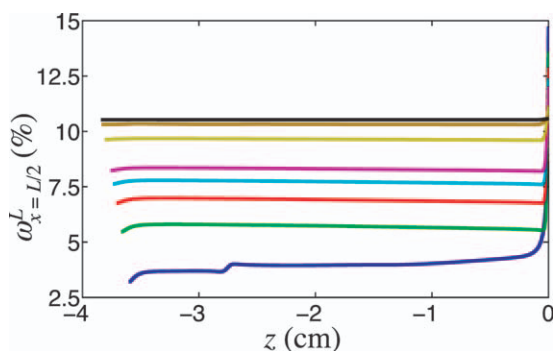


Figure 6. Composition of CO₂ in the middle of the PVT cell, plotted across the liquid bulk phase for various times: $t = 150$ s, 5 min, 7.5 min, 10 min, 12.5 min, 25 min, 52 min, and 2 h, from bottom to top.

The parameters are the same as in Figure 5 and, for the sake of clarity, the results are plotted in the frame of the moving interface, located at $z = 0$. [Color figure can be viewed in the online issue, which is available at wileyonlinelibrary.com.]

The 2-D composition field at different stages of the mixing is shown in Figure 7 for the liquid phase. Convection starts off close to the lateral boundaries of the PVT cell in the liquid

region near the interface, 3 s after the liquid and the gas phases are brought into contact. Because of the sharp difference between the interfacial and bulk compositions, as seen in Figure 6, the interface is not shown to have a better color contrast. The composition field is initially symmetric about the middle of the PVT cell. After 26 s of mixing, two fingers, mirror images of each other, initiate at the interface close to the symmetry line and merge rapidly into one sinking finger. After 36 s, the symmetry breaks and the finger starts traveling toward the left side of the cell. From that moment up to the time when the system reaches equilibrium, the dynamics is complex with one finger originating at a random position of the interface, most often close to the center of the system, and sinking in the bulk. At the same time, the base of the finger propagates along the interface toward either the left or the right boundary, leading to pronounced downflow at the sides. The last five panels of Figure 7 illustrate one case of a finger traveling to the left. In the early stages of mixing, a new finger appears every 10–30 s while it can take up to several minutes at longer times when the system gets close to equilibrium. The velocity field in the liquid phase, including the interface, is illustrated in Figure 8 at times corresponding to the first, third, fifth, and seventh panels of Figure 7. The maximum velocity is about 1 cm/s and the fluid circulation slows down with time. We note that this dynamics is quite different from the density-driven

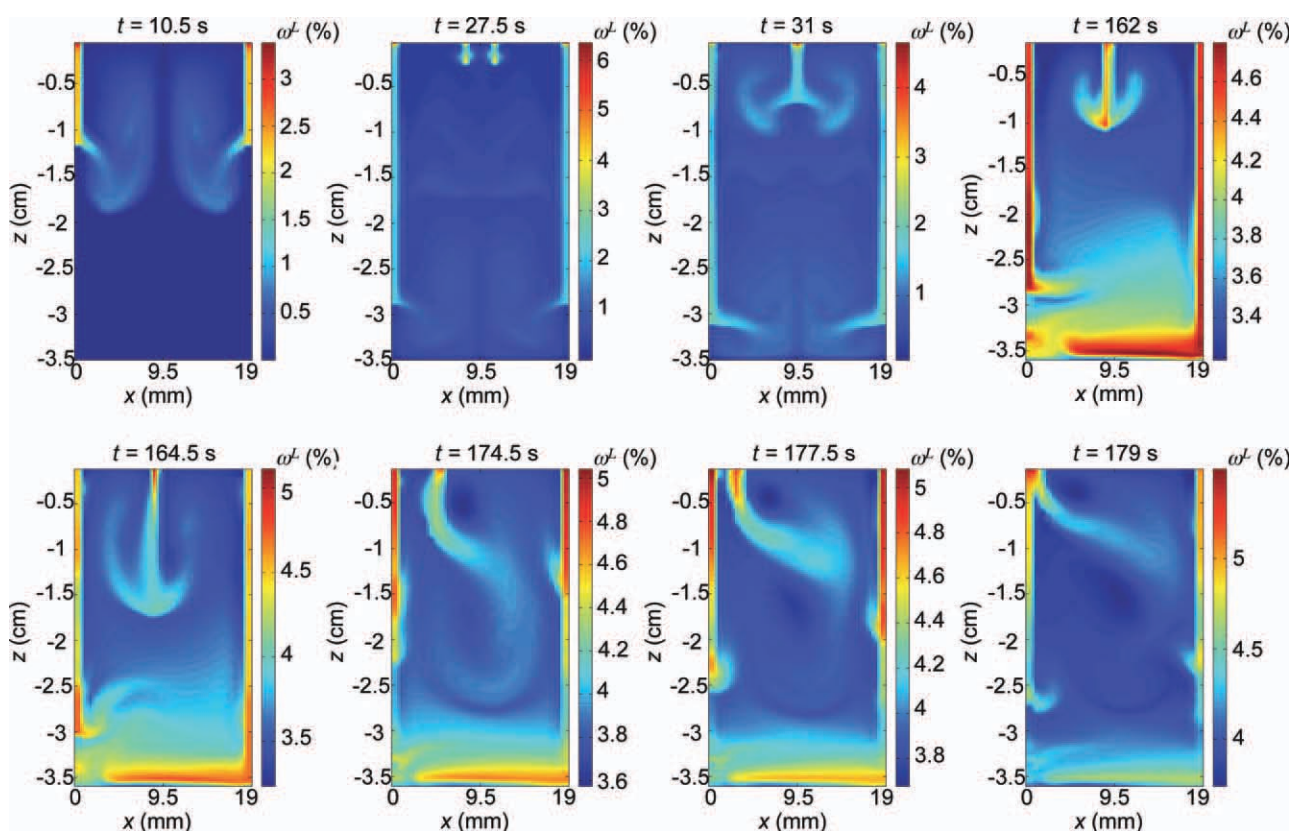


Figure 7. Liquid CO₂ composition for various times: $t = 10.5, 27.5, 31, 162, 164.5, 174.5, 177.5,$ and 179 s, from left to right and top to bottom.

For better color contrast, the interface is not represented and the color scale has been optimized for each panel. The first three panels illustrate the initially symmetric dynamics. The last five panels are illustrative of the dynamics occurring for most of the mixing. Besides important downward flow at the sides, one finger keeps initiating randomly along the interface. Its subsequent motion is downward and toward one of the lateral sides of the PVT cell. All the conditions are the same as in Figure 5 and the results are plotted in the frame of the moving interface, located at $z = 0$. [Color figure can be viewed in the online issue, which is available at wileyonlinelibrary.com.]

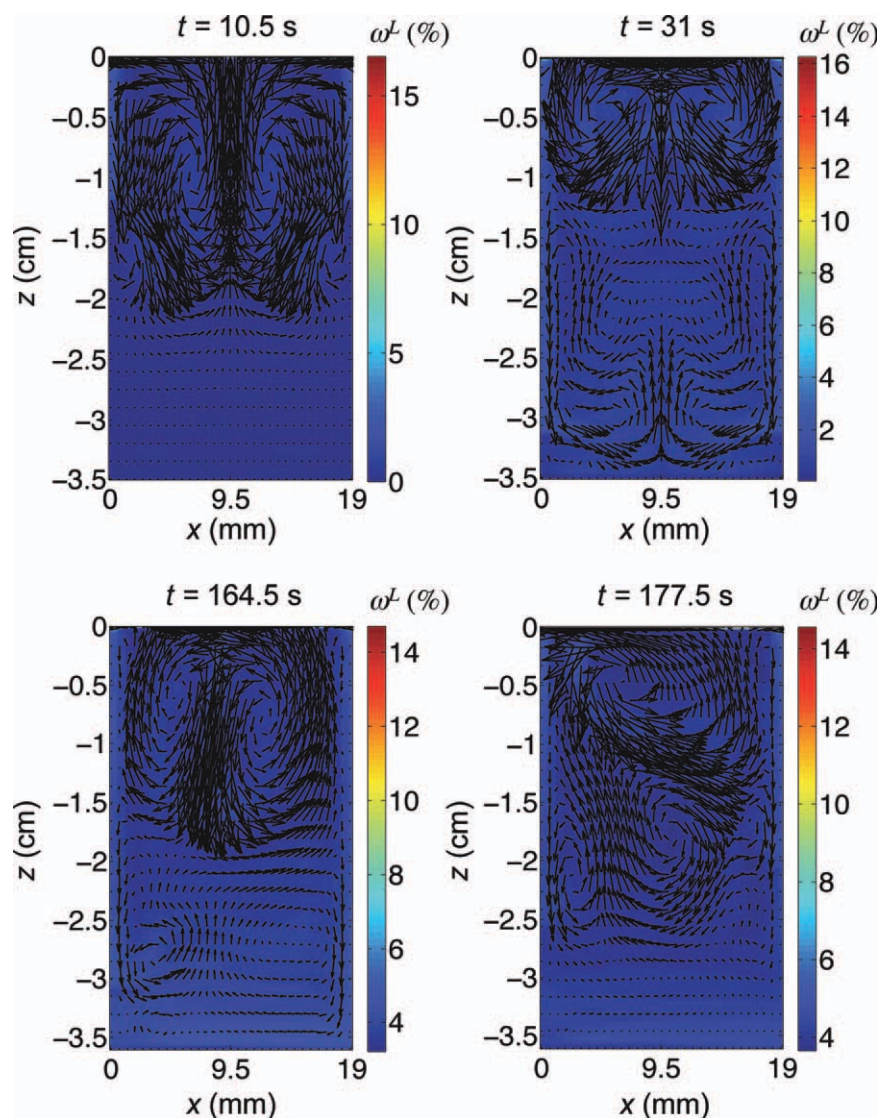


Figure 8. Velocity field in the liquid phase, including the interface, superimposed on the composition field of CO₂ for various times: $t = 10.5, 31, 164.5,$ and 177.5 s, from left to right and top to bottom (times corresponding to the first, third, fifth, and seventh panels of Figure 7).

All the conditions are the same as in the previous figure and the results are plotted in the frame of the moving interface, located at $z = 0$. The arrows, however, represent the real length of the velocity vectors in the fixed frame. The maximum velocity is about 1 cm/s and decreases with time. [Color figure can be viewed in the online issue, which is available at wileyonlinelibrary.com.]

fingering observed in porous media or Hele-Shaw cells where the initial convective patterns consist in fingers with a well-defined wavelength^{6,16,17} and evolving in time by coarsening or tip splitting.

In the gas phase, a couple of convection rolls is initiated by viscous drag at the interface and dies out in the bulk.

Mass Fluxes

We analyze the diffusive mass flux, $\vec{J}_D = -\rho D \nabla \omega$, and the convective mass flux, $\vec{J}_C = \rho \omega \vec{v}$, both in the liquid bulk phase and at the interface, to highlight the transport processes controlling the mixing. Figure 9a displays the maximum intensity of the vertical diffusive and convective mass fluxes at the

liquid side of the interface. The diffusive flux is always an order of magnitude larger than the convective flux and is negative, transferring CO₂ from the interface to the liquid phase. This points out that diffusion dominates the mass transfer at the interface, and explains our results sensitivity to the diffusion coefficient (see Figures 2 and 3), allowing us to measure accurate value even if convection has a huge effect on the mixing time scale (see Figure 4). Indeed, the maximum intensity of the diffusive and convective fluxes in both directions inside the liquid bulk phase, plotted in Figure 9b, indicates that the mixing in the bulk takes place mostly by convection. Both types of fluxes decrease by several orders of magnitude during the mixing, at the interface as well as in the bulk after a significant increase in the very short times.

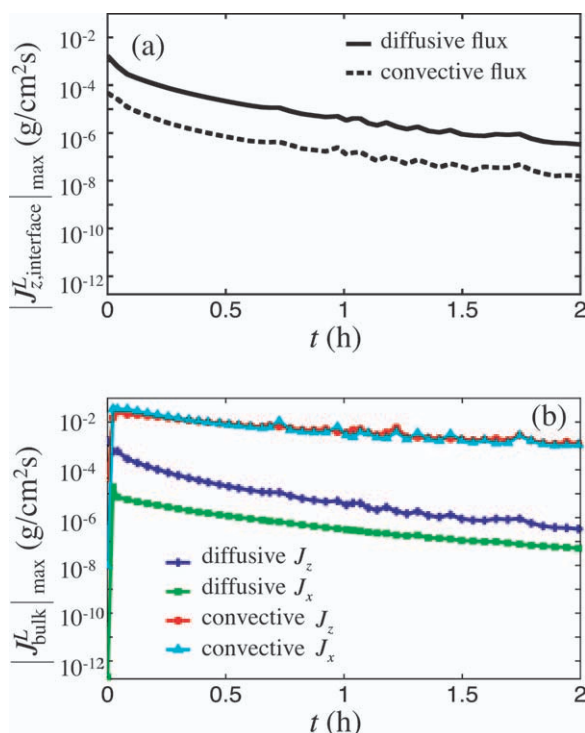


Figure 9. Maximum intensity of the diffusive and convective vertical fluxes (a) on the liquid side of the interface as a function of time and (b) in the liquid phase, both in the vertical and in the horizontal directions, as a function of time.

The plots are on a semi-log scale to accurately represent the changes by several orders of magnitude during the mixing. All the parameters are the same as in the previous figures. [Color figure can be viewed in the online issue, which is available at wileyonlinelibrary.com.]

Concluding Remarks

When two non equilibrium gas and liquid phases are brought into contact, mass transfers across the interface until partial or complete mixing is achieved. We have studied the case of a binary mixture formed by CO₂ and normal decane, pointing out that natural convection, triggered by the density increase of the liquid phase upon dissolution of CO₂, accelerates the mixing between the two phases by a factor 50 for typical experimental conditions (total density increase in the liquid phase, $\Delta\rho^L = 0.01 \text{ g/cm}^3$). Because of this very efficient mixing, the liquid bulk composition is almost uniform. At the interface, however, the diffusive fluxes control the supply of CO₂, which is demonstrated by the sensitivity of the results to the diffusion coefficients. The model presented here aims at representing the different processes accurately so that a comparison with experimental data can allow for the measurement of the diffusion coefficients. Our 2-D model includes Fickian diffusion, convective mass transport arising from compressibility, non ideality, and natural convection in both phases. The motion of the interface upon mixing is incorporated in the model, the fluid properties are calculated with the Peng-Robinson

equation of state, and the diffusion coefficients vary with pressure and composition.

We have considered a 2-D model. Three-dimensional-effects that may influence the dynamics described here are beyond the scope of this article. In 2-D, we include all the physical processes in the experimental system in our description. The assumption of a non deformable interface can be justified by considering the dimensionless capillary number, measuring interfacial deformation, $Ca = \mu U/\gamma$, where U is a characteristic speed and γ is the interfacial tension between CO₂ and nC₁₀. Interfacial tension in a CO₂-nC₁₀ system at similar conditions as ours, $T = 310.85 \text{ K}$ and $P = 28 \times 10^5 \text{ Pa}$, has been obtained from equilibrium measurements¹⁸ and is around $16 \times 10^{-3} \text{ N/m}$. Using the viscosity of the liquid phase, $\mu^L = 71.26 \times 10^{-5} \text{ Pa s}$ (see Table 1), and its characteristic velocity at the early stages of mixing, $U \sim 1 \text{ cm/s}$, leads to the maximum capillary number for our system, $Ca = 4.5 \times 10^{-4}$. We can therefore safely neglect any surface deflections.

Extending this work to mixtures with more than two components and accounting for variable viscosity is a further step to consider to determine diffusion coefficients in multi-component systems for which data are very scarce. The mixing between CO₂ and water is a very important and timely issue that could also be addressed with our model adapted to polar mixtures by changing the equation of state.¹⁹

Acknowledgments

The authors acknowledge financial support from the member companies of R.E.R.I., and L.R. is supported by the F.R.S.-F.N.R.S. Belgium. They also thank the Instituto Mexicano del Petroleo for sharing their experimental data.

Literature Cited

- Moortgat J, Firoozabadi A. Higher-order compositional modeling with Fickian diffusion in unstructured and anisotropic media. *Adv Water Resour.* 2010;33:951–968.
- Schrag DP. Preparing to capture carbon. *Science.* 2007;315:812–813.
- Firoozabadi A, Cheng P. Prospects for subsurface CO₂ sequestration. *AICHE J.* 2010;56:1398–1405.
- Lindeberg E, Wessel-Berg D. Vertical convection in an aquifer column under a gas cap of CO₂. *Energy Convers Manage.* 1997;38:229–234.
- Ennis-King J, Preston I, Paterson L. Onset of convection in anisotropic porous media subject to a rapid change in boundary conditions. *Phys Fluids.* 2005;17:084107.
- Riaz A, Hesse M, Tchelepi HA, Orr FM. Onset of convection in a gravitationally unstable diffusive boundary layer in porous media. *J Fluid Mech.* 2006;548:87–111.
- Kneafsey TJ, Pruess K. Laboratory flow experiments for visualizing carbon dioxide-induced, density-driven brine convection. *Transp Porous Med.* 2010;82:123–139.
- Farajzadeh R, Zitha PLJ, Bruining J. Enhanced mass transfer of CO₂ into water: experiment and modeling. *Ind Eng Chem Res.* 2009;48:6423–6431.
- Nepomnyashchy AA, Velarde MG, Colinet P. *Interfacial Phenomena and Convection.* Boca Raton: Chapman and Hall/CRC, 2002.
- Leahy-Dios A, Firoozabadi A. Unified model for nonideal multicomponent molecular diffusion coefficients. *AICHE J.* 2007;53:2932–2939.
- Peng D-Y, Robinson DB. New 2-constant equation of state. *Ind Eng Chem Fundam.* 1976;15:59–64.
- Haugen KB, Firoozabadi A. Mixing of two binary nonequilibrium phases in one dimension. *AICHE J.* 2009;55:1930–1936.

13. Haugen KB, Firoozabadi A. Composition at the interface between multicomponent nonequilibrium fluid phases. *J Chem Phys.* 2009;130:064707.
14. Taylor R, Krishna R. *Multicomponent Mass Transfer*. New York: Wiley, 1993.
15. Reamer HH, Sage BH. Phase equilibria in hydrocarbon systems. Volumetric and phase behavior of the n-decane-CO₂ system. *J Chem Eng Data.* 1963;8:508–513.
16. Manickam O, Homsy GM. Fingering instabilities in vertical miscible displacement flows in porous media. *J Fluid Mech.* 1995;288:75–102.
17. Moortgat J, Sun S, Firoozabadi A. Compositional modeling of three-phase flow with gravity using higher-order finite element methods. *Water Resour Res.* 2011;47:W0511.
18. Ayirala SC, Rao DN. Miscibility determination from gas–oil interfacial tension and P-R equation of state. *Can J Chem Eng.* 2007;85:302–312.
19. Li ZD, Firoozabadi A. Cubic-plus-association equation of state for asphaltene precipitation in live oils. *Energ Fuel.* 2010;24:2956–2963.

Manuscript received Sept. 3, 2010, and revision received Apr. 18, 2011.